creative commons

COMMONS DEED

저작자표시-비영리-변경금지 2.0 대한민국

이용자는 아래의 조건을 따르는 경우에 한하여 자유롭게

- 이 저작물을 복제, 배포, 전송, 전시, 공연 및 방송할 수 있습니다.

다음과 같은 조건을 따라야 합니다:

저작자표시. 귀하는 원저작자를 표시하여야 합니다.

비영리. 귀하는 이 저작물을 영리 목적으로 이용할 수 없습니다.

변경금지. 귀하는 이 저작물을 개작, 변형 또는 가공할 수 없습니다.

- 귀하는, 이 저작물의 재이용이나 배포의 경우, 이 저작물에 적용된 이용허락조건을 명확하게 나타내어야 합니다.
- 저작권자로부터 별도의 허가를 받으면 이러한 조건들은 적용되지 않습니다.

저작권법에 따른 이용자의 권리는 위의 내용에 의하여 영향을 받지 않습니다.

이것은 이용허락규약(Legal Code)을 이해하기 쉽게 요약한 것입니다.

Disclaimer

dCollection

공학석사 학위논문

Alteration of Low Density Operation Range by Resonant Magnetic Perturbation in KSTAR

KSTAR의 자기공명섭동에 의한
저밀도 운전영역의 변화에 관한 연구

2016년 **2**월

서울대학교 대학원

에너지시스템공학부

손 정 훈

Alteration of Low Density Operation Range by Resonant Magnetic Perturbation in KSTAR

지도교수 나 용 수

이 논문을 공학석사 학위논문으로 제출함

2016년 2월

서울대학교 대학원

에너지시스템공학부

손 정 훈

손정훈의 석사 학위논문을 인준함

2016년 2월

위 원 장 황 용 석 (인)

부위원장 나 용 수 (인)

위 원 인 용 균 (인)

Abstract

Alteration of Low Density Operation Range by Resonant Magnetic Perturbation in KSTAR

Son, Jeong-hoon
Department of Energy System Engineering
The Graduate School
Seoul National University

Knowing the operation range of tokamak is important since the operation parameters determine the fusion output power and plasma operation scenarios. In this thesis the operation range of KSTAR was revealed via Hugill diagram and Greenwald density fraction diagram. In total 1740 experimental shots were selected carefully for this analysis which were performed from 2011 to 2014 in KSTAR. By comparing the operation range of KSTAR with that of DIII-D via Hugill diagram, it was found that KSTAR can reach far lower density, insisting that KSTAR has extremely low intrinsic error field. The range of the achievable Greenwald fraction of KSTAR was shown to be 6% to 60% in the present database.

The two factors, runaway electron and error field, which can alterate

the achievable low density operation range were investigated. The condition for the generation of the runaway electron in KSTAR was found via Dreicer condition with dedicated runaway electron generation experiments. Although these experiments satisfy the condition for generating runaway electrons, all of these shots could be sustained without significant interruptions. Based on this observation the runaway electrons are not thought to be the main factor to set the low density operation limit in KSTAR. On the other hand, plasma shots with the increased error field by applying the resonant magnetic perturbation(RMP) often showed the plasma locking phenomenon so that access to the low density operation range was significantly constrained. The plasma locking threshold is found to be differed by the position of the applied RMP coil and the q_{95} value. The RMP coil current magnitude needed for plasma locking from the middle coil is about half of that from the top or the bottom coil. And the lower q_{95} value showed the lower density operation range, with $f_{GW} \approx 0.16$ in $q_{95} = 3.2$ cases and $f_{GW} \approx 0.22$ in $q_{95} = 4.4$ cases. The influence of RMP to the low density range is investigated in terms of the L-mode to H-mode transition power which shows that access to the optimal density range of the L-H transition can be limited by applying RMP. Therefore, it is suggested to take this effect into account in designing operation scenarios for tokamaks employing RMP to suppress edge localized modes in H-mode plasmas in particular.

keywords: KSTAR, Density limit, Hugill diagram, Greenwald density fraction, Resonant magnetic perturbation, Runaway electron, tokamak operation

Student Number : 2013-23182

Contents

Abstract i
Contents iv
List of Figures vi

Chapter 1 Introduction 1
1.1 Motivation 1
1.2 Preceding researches 2
1.2.1 Operation limit 2
1.2.2 Physics background of the low density limit 3
1.3 Purpose of this study 4

Chapter 2 Operation range of KSTAR 7
2.1 Data acquisition 7
2.2 Operation range of KSTAR 11

Chapter 3 Alteration of low density operation range 14
3.1 Effect of runaway electrons 14
3.2 Effect of resonant magnetic perturbation (RMP) 16
3.2.1 RMP application in KSTAR 16
3.2.2 Types of plasma locking 17
3.2.3 Several features of locked plasmas 19
3.2.4 Low density limit change by RMP 22
3.2.5 Impact to L-H power threshold by RMP 24

Chapter 4 Conclusion 26

References ····· 28
국문 초록 ····· 31

List of Figures

Figure 1.1 Hugill diagram [3] ····· 2
Figure 1.2 L-H transition power threshold in KSTAR with the experiments in 2010 and 2011[2] ····· 5

Figure 2.1 Example of selecting 5 time points (green) in the plasma flattop (red) (#9197) ····· 8
Figure 2.2 Excluded shot due to data shortage of minor radius, major radius and elongation. The data lack area is indicated by green boxes (#5899) ····· 9
Figure 2.3 Excluded shot due to continuous density rising (green area) caused by fringe jump error (#8035) ····· 10
Figure 2.4 (a) The operation range of KSTAR via Hugill diagram, (b) Comparison of the operation range of KSTAR with DIII-D [9] ····· 12
Figure 2.5 The operation range of KSTAR via Greenwald density limit and the Greenwald density fraction ····· 13

Figure 3.1 Overview of the dedicated runaway electron plasma (#7598) ····· 14
Figure 3.2 The position of the dedicated runaway electron shots on Hugill diagram ····· 15
Figure 3.3 (a) Configuration of the KSTAR In-Vessel control coils, (b) Schematic diagram of the In-Vessel control coils and field error correction coils [13] ····· 16
Figure 3.4 Possible configurations of the RMP phase [14] ··· 17

Figure 3.5 Two cases of plasma locking: (a) Locking with H-L back-transition and subsequent disruption when RMP applied in H-mode plasmas (#9063) which is compared with a no RMP case (#9064), (b) Locking over threshold RMP coil current in L-mode plasmas (#8856) ····· 18
Figure 3.6 Overview of #8973 with plasma locking point ····· 19
Figure 3.7 MHD spectrogram of #8973 ····· 20
Figure 3.8 Evolution of the temperature profile in time; t = 2.4 s (black), t = 2.7 s (red), t = 3 s (blue) t = 3.3 s (green) and t = 3.6 s (magenta) ····· 21
Figure 3.9 Plot of the locking points in Greenwald fraction and RMP coil current window ····· 22
Figure 3.10 Plot of the plasma locking points shown in Figure 3.9 with Hugill diagram and Greenwald fraction diagram ····· 23
Figure 3.11 Diagram of plasma locking range over L-H threshold power versus Greenwald density fraction for (green) and (violet) ····· 25

Chapter 1 Introduction

1.1 Motivation

In nuclear fusion research for developing fusion power plants, finding out the operation range of a tokamak device, especially with respect to the plasma density is important for tokamak operations since the operation range can influence the fusion performance of a tokamak.

The so-called density limit can be subdivided into the upper density limit and the low density limit. The upper density limit affects the fusion power output, since the fusion reaction rate is known to be proportional to n^2[1]. Therefore, many studies about operation range have been focused on upper density limits, since the output fusion power is directly related to maximum density. But the low density limit can also affect the fusion performance in terms of the L-mode to H-mode (L-H) transition power threshold. In many devices, optimal density exists where the L-H transition power exhibits the lowest value. If this density can not be accessed due to the low density limit, more heating power will be needed to achieve H-modes so that the fusion power multiplication factor (Q) could be reduced and more power will be needed for a fusion reactor. Therefore, in this thesis, the operation range will be investigated, mostly in view of this low density limit.

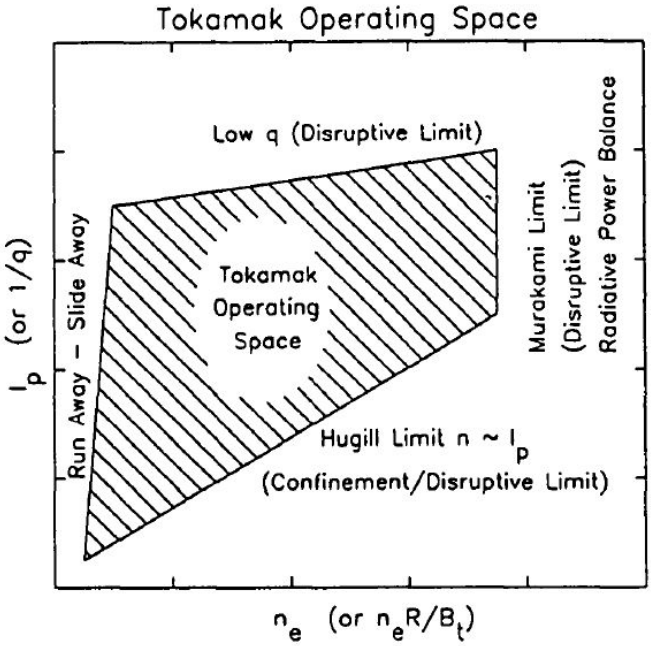

Figure 1.1 Hugill diagram [3]

1.2 Preceding researches

1.2.1 Operation limit

The operational range can be characterized by Hugill diagram[3], as shown in Figure 1.1. The Hugill diagram was originally set by collecting experimental data from several tokamaks. Each boundary of the diagram represents its own condition for density limit. The left-hand side is the low density limit, usually set by runaway electrons. The upper side is limited by the plasma current limit at low safety factor. The righthand side is set by the power balance between the input power and the plasma radiation. The lower part is the plasma confinement limit between the plasma density and the

plasma current, represented as Hugill limit[4][5]. The Hugill limit is later replaced by the Greenwald density limit, expressed as $n_{GW} = I_P/\pi a^2$. The Greenwald density limit indicates the maximum achievable density in each tokamak. But later the condition for the density limit is known to related with the edge plasma density only, so one can exceed the Greenwald density limit by plasma shaping, central fuelling, edge pumping, and others.

1.2.2 Physics background of the low density limit

The low density limit can be set by several reasons. One is by the runaway electrons, as mentioned in Hugill diagram. Early experiments of tokamak showed the disruptions in low density operation because of massive impurities generated by runaway electron[6][7]. The condition for generating runaway electron is determined by the Dreicer's model[8]. In this model, the runaway electron can be generated over the critical electric field, $E > E_c$,, where $E = V_{loop}/2\pi R$ and $E_c = \dfrac{nq^2 \ln \Lambda}{4\pi\epsilon_0^2 mc^2} \cong 0.08 n_{20}$ with assuming $\ln \Lambda \approx 15$. So it is expected that the number of runaway electrons will increase as the density goes down.

Another reason for the low density limit is the plasma locking due to error fields. We consider two types of error fields in this thesis. The first one is the intrinsic error field. Every tokamak has the intrinsic error field because of the imperfection of the coil symmetry.

The low density limit set by the intrinsic error field was studied in DIII-D[9]. In this study, the large intrinsic error field in DIII-D induced plasma locking, hence resulting in increase of the low density limit. This phenomenon was mitigated by applying additional magnetic fields to compensate the error field, the so-called error field correction. The other is the resonant magnetic perturbation (RMP). The RMP can affect the plasma rotation, density, and so on. Especially, large magnitude of RMP is known to induce plasma locking and disruptions.

1.3 Purpose of this study

The Korea Superconducting Tokamak Advanced Researches (KSTAR) device was constructed and achieved the first plasma in 2008. It aims at achieving long-pulse high performance steady-state plasma operations.

A variety of researches have been made to investigate the tokamak operation range with the density limits in several tokamak machines, however KSTAR has not addressed this yet. In this thesis, the operation range of KSTAR will be investigated. Particular focus will be upon the explanation of the low density limit identified in KSTAR.

The intrinsic error field of KSTAR was investigated recently, insisting that the KSTAR has an extremely low intrinsic error field compared to other tokamak devices[10]. In this point of view, KSTAR is expected to have little influence of error field to determination of the low density limit.

On the other hand, the effect of the runaway electrons and the error field by RMP is not clearly revealed yet. Furthermore, the RMP is generally used to suppress edge localized mode in H-mode plasmas and to study the neoclassical toroidal viscosity. Many experiments using RMP have been performed in KSTAR and lots of plasma shots showed plasma locking and sometimes disruptions when RMP applied during experiments.

The L-H transition power threshold is investigated using the database collected from experiments performed in 2010 and 2011 of the KSTAR campaign, and the result is shown in Figure 1.2[2]. From this result, one can see there is an optimal density for efficient L-H transition with the lowest auxiliary heating power in KSTAR. Assuming that this phenomenon can be projected to a fusion reactor if the density cannot reach this region by several reasons, the heating power for L-H threshold must be increased, and it can affect the fusion amplification factor.

In conclusion, the operation range and the effect of the runaway electron and the RMP to the low density limit in KSTAR will be revealed in this thesis. In chapter 2, the preparation process for plotting the Hugill diagram will be introduced first, then the overall operation range of KSTAR will be introduced via Hugill diagram and the Greenwald density fraction. The effect of runaway electron and the RMP to low density limit will be discussed in chapter 3. Summarization of the results and conclusions will be drawn in chapter 4.

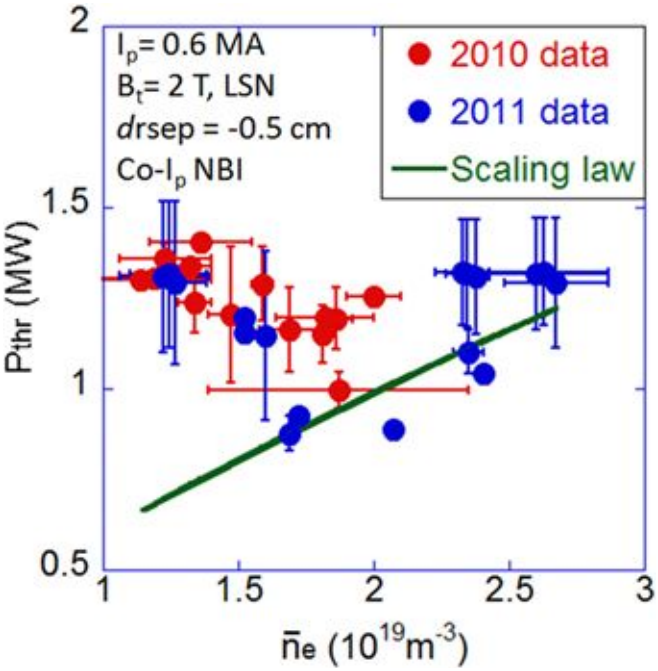

Figure 1.2 L-H transition power threshold in KSTAR with the experiments in 2010 and 2011[2]

2. Operation range of KSTAR

2.1 Data acquisition

To investigate the operation range of KSTAR, experiment results from 2011 to 2014 of plasma shots were collected. The range of the plasma shots performed during this period covers from shot 4469 to shot 11726. Five points were selected per shot during the flattop of the plasma. The selection process of the data time points is as follows:

① Smooth the plasma current in time

② Find the both ends of the current flattop - set as 0 and 1

③ Set the half point of both end - 0.5

④ Set the half point between ③ and each end - 0.25 and 0.75

⑤ Set the half point between ③ and ④ - 0.375 and 0.675

An example of the selected points is shown in Figure 2.1 of shot 9197. The physics parameters needed to plot Hugill diagram were calculated on these time points by interpolation. All these processes were conducted by using MATLAB code to handle the large amount of data.

During these processes, it is found that not all the shots were suitable for analysis. The cases of unsuitable data can be categorized as follows.

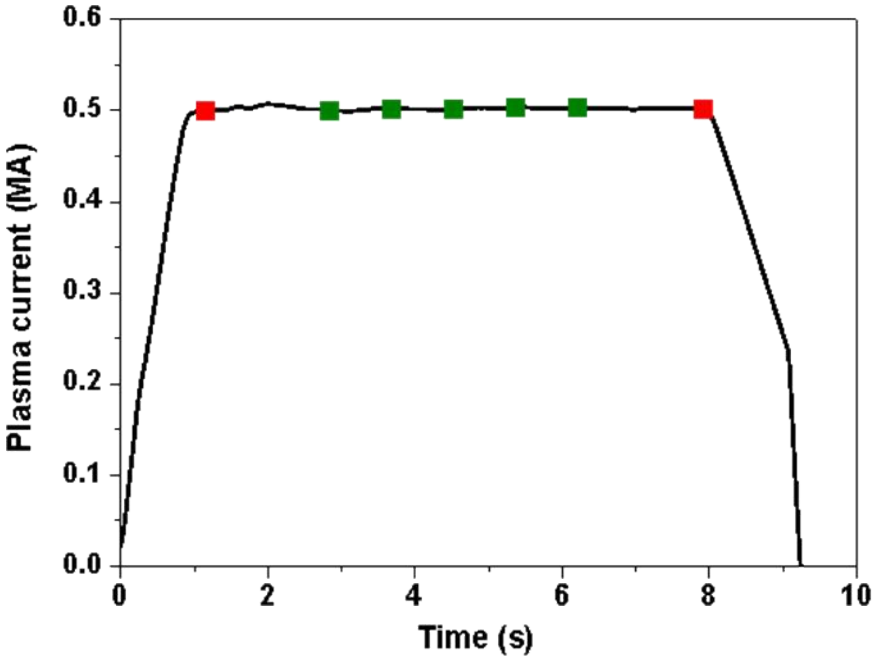

Figure 2.1 Example of selecting 5 time points (green) in the plasma flattop (red) (#9197)

The first case is the data shortage of the plasma shots. Most of this case includes the missing of the critical data for analyses, such as the plasma density or the plasma current, which are needed to calculate for plotting the Hugill diagram. Some shots have the data lack in part of the pulse. A typical example of this case is shown in Figure 2.2 of the shot 5899 where the three data, minor radius, major radius, elongation data were cut-off during the plasma flattop phase, which causes error in the interpolation process.

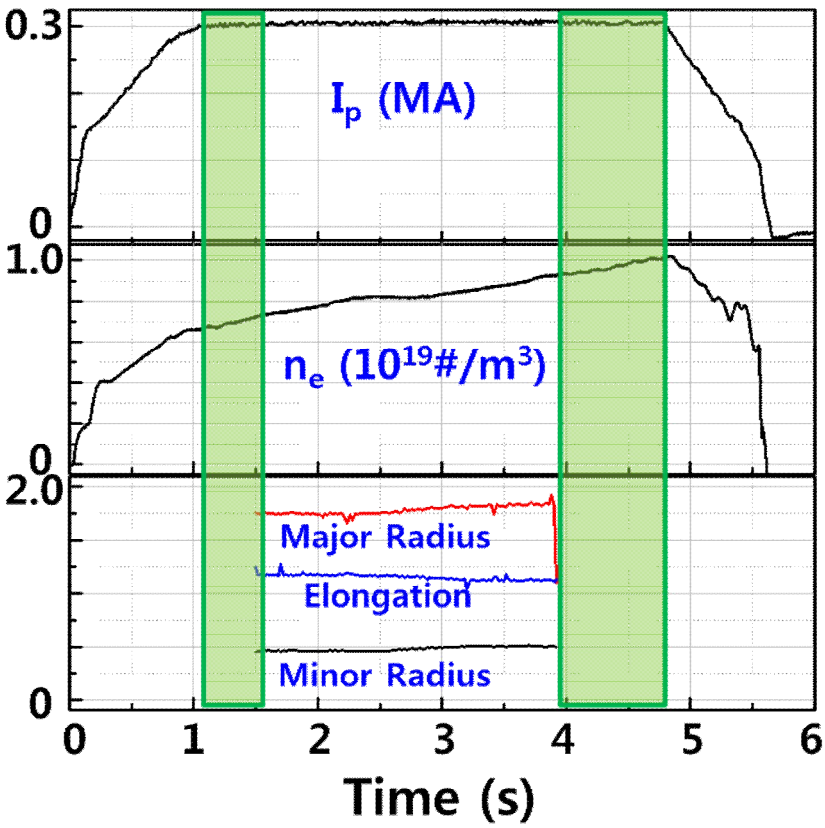

Figure 2.2 Excluded shot due to data shortage of minor radius, major radius and elongation. The data lack area is indicated by green boxes (#5899)

The second case is the improper data measurements or calculations. Most of this case is caused by density profile. In KSTAR the 280 GHz millimeter wave interferometer is used to measure the electron line average density[11]. Since the interferometer has the possibility of the fringe jump error, the advanced method[12] is used to reduce this fringe jump error to get more accurate density. However, some of

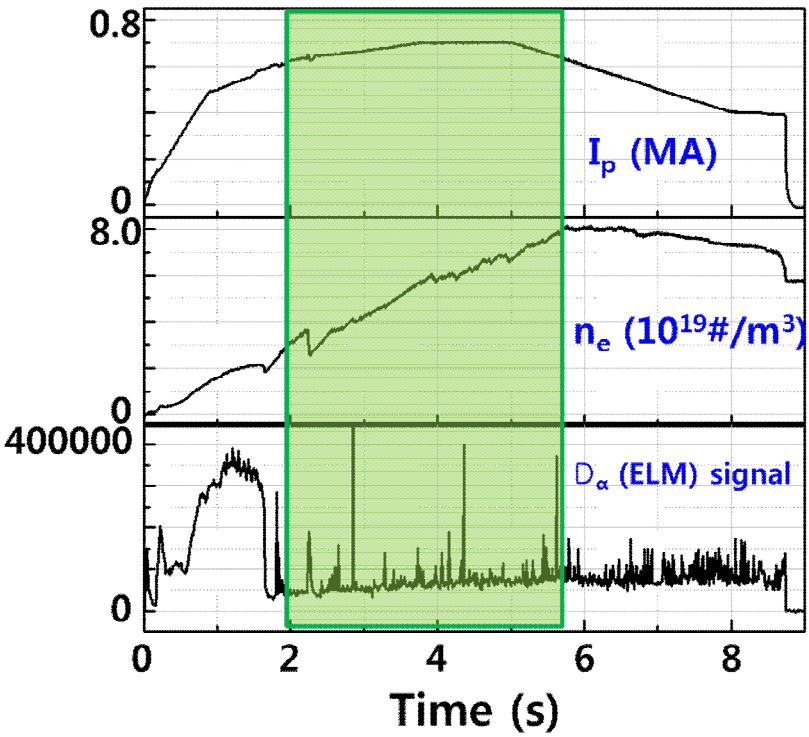

Figure 2.3 Excluded shot due to continuous density rising (green area) caused by fringe jump error (#8035)

the plasma shots showed the continuous density rising. The typical case is shown in Figure 2.3 of shot 8035. This phenomenon usually appeared in the H-mode phase with the ELM activity.

Since these unsuitable data can significantly affect the analysis result, shots were carefully selected by excluding these unsuitable shots.

From this data refining process, totally 2593 shots were obtained. Among them, 853 shots showed the disruption during the plasma

flattop, while the remaining 1740 shots were sustained without disruptions.

2.2 Operation range of KSTAR

The operation range of KSTAR was investigated via Hugill diagram and Greenwald density fraction range, with the 1740 shots which were not disrupted. The three data, the minor radius, the major radius and the elongation, are taken from the real-time equilibrium reconstruction (rt-EFIT). The minor radius and the major radius are kept the same value, averaged over the current flattop phase, at all the selected time points in each shot to mislead results due to non-physical oscillations frequently observed in raw data.

Figure 2.4(a) shows the operation range of KSTAR via Hugill diagram which is compared with that of DIII-D in General Atomics in the U.S.A. [9] is shown in Figure 2.4(b). The shifted position of the diagram is thought mainly due to the difference of the toroidal magnetic field (B_T) as DIII-D is about 1-2 T referred to 1.5-3.8 T of KSTAR. Nonetheless, KSTAR can reach far low density than DIII-D which is thought to be result from extremely low intrinsic error field of KSTAR [8]. This will be discussed in more detail below.

Figure 2.5 shows the operation range plotted with Greenwald fraction diagram in 'n_{GW} vs n_e'. In this diagram the gradient can be directly expressed in the Greenwald density fraction. The maximum value of the Greenwald fraction showed 80%, but considering the

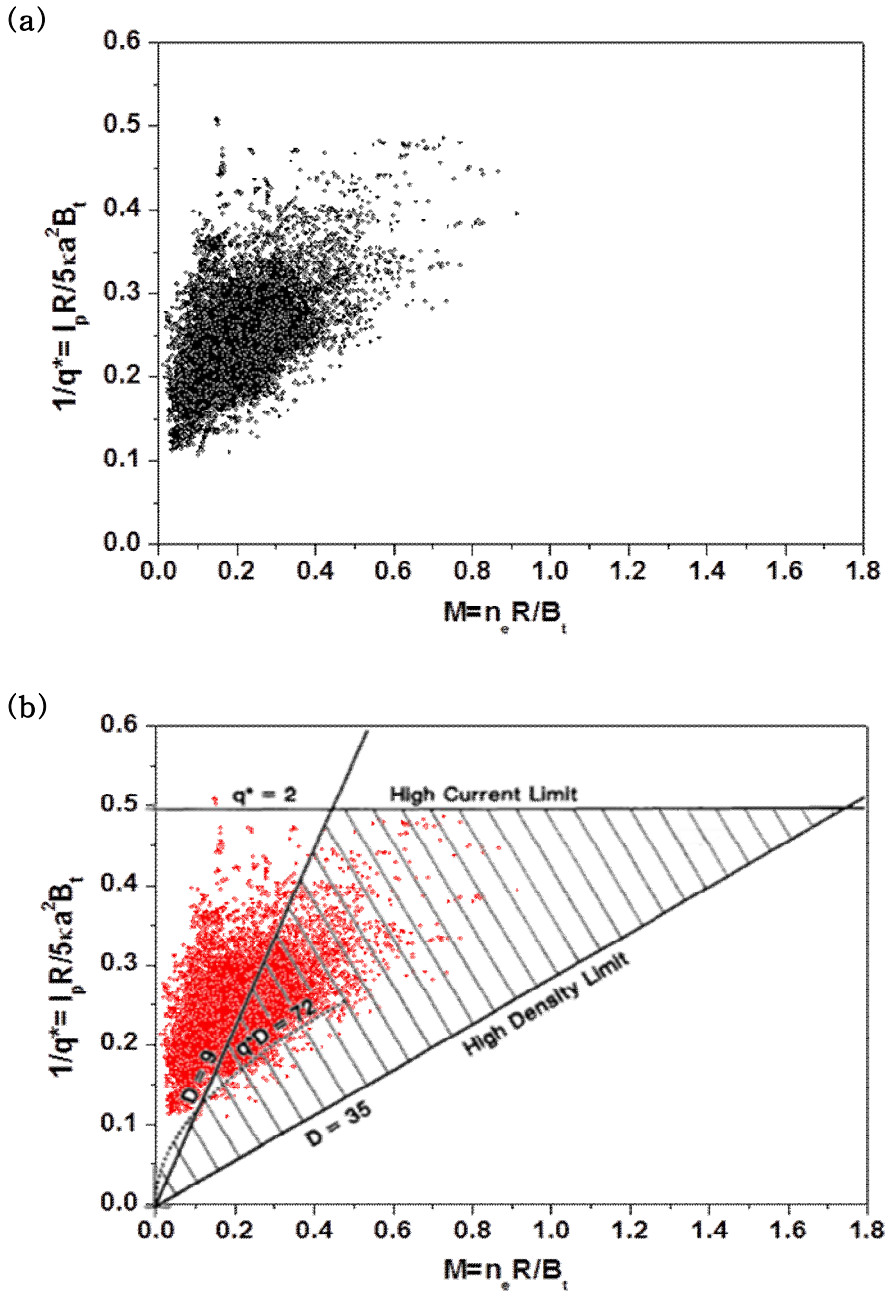

Figure 2.4 (a) The operation range of KSTAR via Hugill diagram, (b) Comparison of the operation range of KSTAR with DIII-D[7]

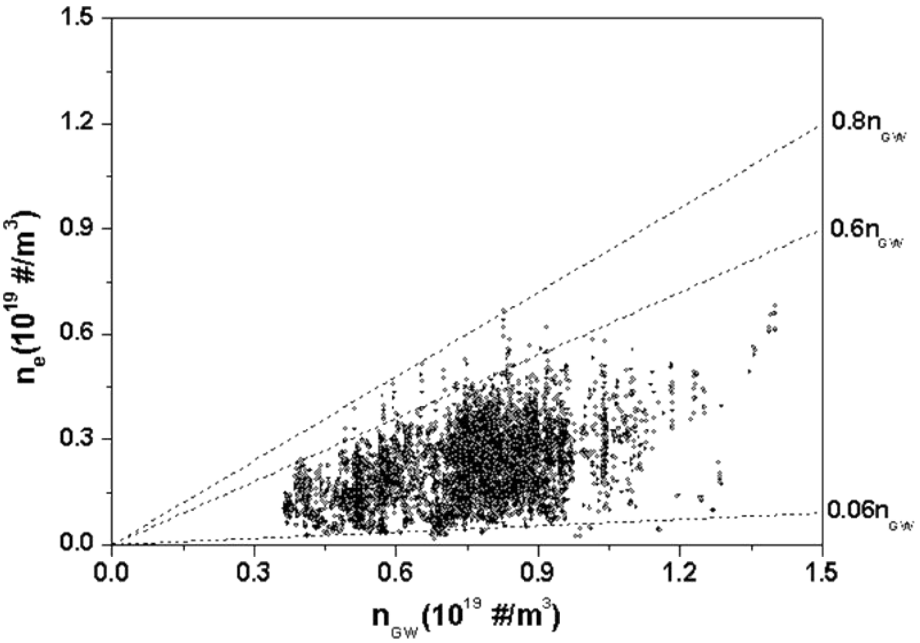

Figure 2.5 The operation range of KSTAR via Greenwald density limit and the Greenwald density fraction

error range of the minor radius in EFIT and the data distribution, which is thought to be about 60%. From the two diagrams with Hugill and Greenwald fraction, it seems that the KSTAR has not enough auxiliary power to reach the maximum Greenwald density limit, resulting in the lack of data in the high density region. In addition, the pellet injection which can increase the core density is not available yet in KSTAR. It is noteworthy that the minimum density is about 6% of the Greenwald fraction.

3. Alteration of low density operation range

3.1 Effect of runaway electrons

The runaway electron is known as the main factor of the low density limit in Hugill diagram[3]. KSTAR also observes the runaway electrons in low density plasmas, especially in $E \geq 5 \times E_c$ condition in view of the Dreicer theory[8]. To check the effect of runaway electron to low density limit, the experiment of the dedicated runaway electron conducted in 2012 were studied. Figure 3.1 is one of the typical

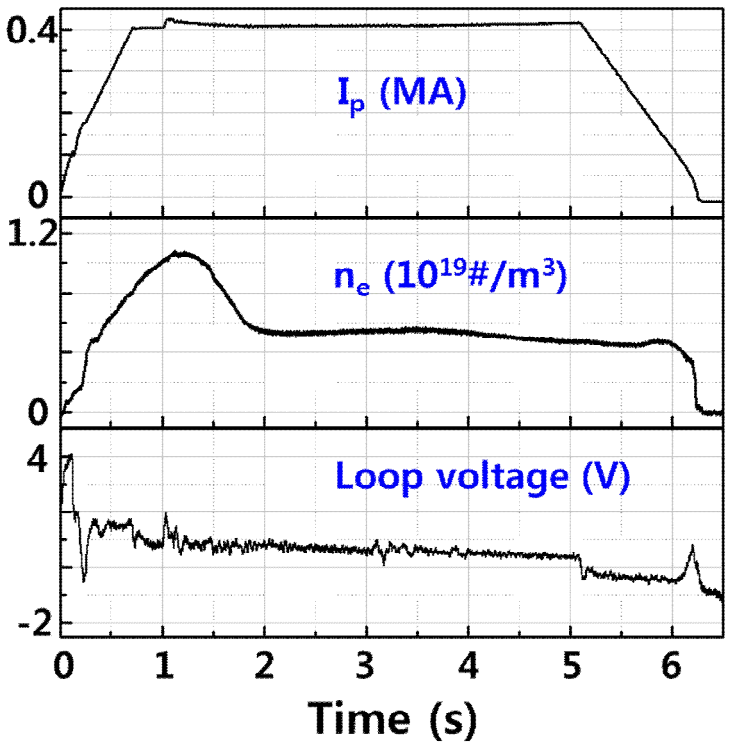

Figure 3.1 Overview of the dedicated runaway electron plasma (#7598)

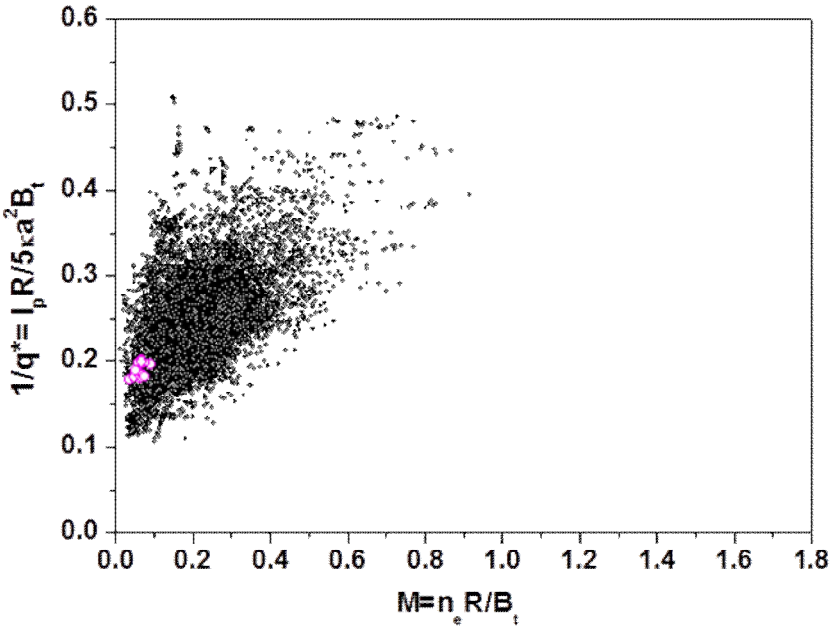

Figure 3.2 The position of the dedicated runaway electron shots on Hugill diagram

runaway electron experiments, and the position of these shots on Hugill diagram is indicated in Figure 3.2. The ratio between the applied electric field and the critical electric field, E/E_c, in these experiments is about 6 to 15. This implies that these shots would produce the runaway electrons. Nevertheless, these shots could be sustained without significant interruptions by the runaway electrons during the plasma current flattop phase. From this result, it is thought that the generation of runaway electron is not the essential factor to set the low density limit.

3.2 Effect of resonant magnetic perturbation (RMP)

3.2.1 RMP application in KSTAR

KSTAR has in-vessel control coils (IVCC) for the purpose of fast plasma position control, field error correction (FEC), and resistive wall mode control [13]. By combining the IVCC, the three pairs of FEC coils can be made in top, middle, and bottom. Combining these coils can produce several RMP phases, as shown in Figure 3.4.

The RMP is widely used in many KSTAR experiments, such as ELM mitigation and suppression, neoclassical toroidal viscosity studies, and others. However, some shots exhibit plasma locking when the RMP is applied.

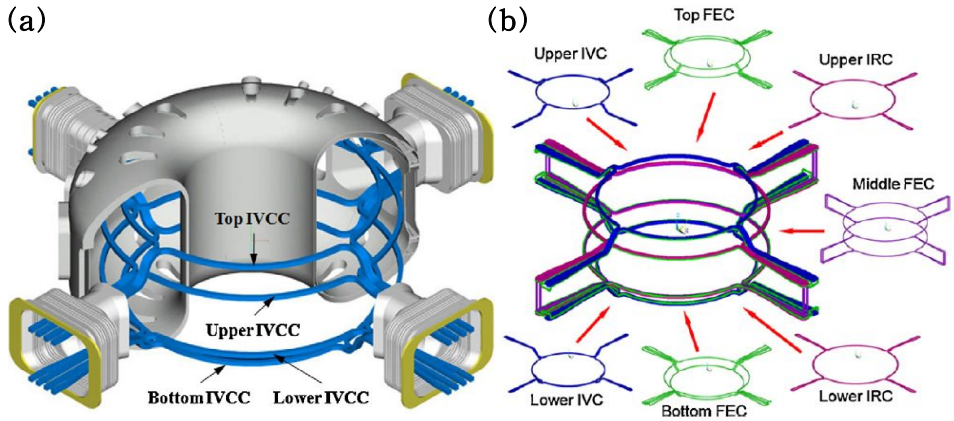

Figure 3.3 (a) Configuration of the KSTAR In-Vessel control coils (b) Schematic diagram of the In-Vessel control coils and field error correction coils [13]

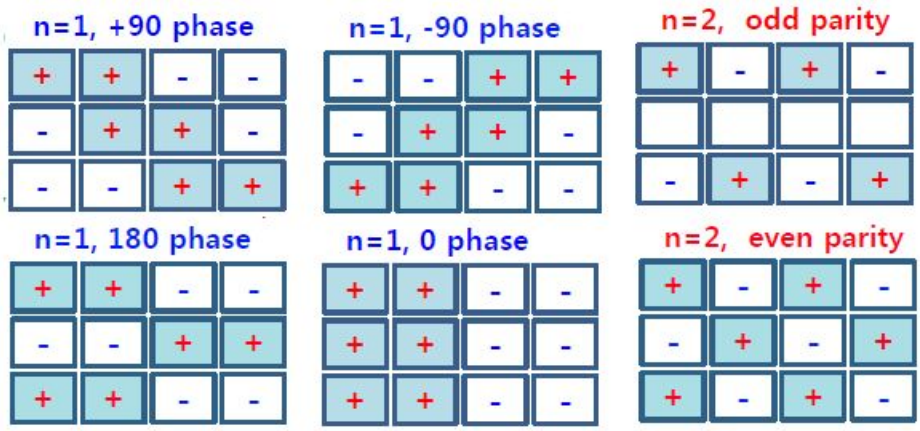

Figure 3.4 Possible configurations of RMP phase [14]

3.2.2 Types of plasma locking

The type of the plasma locking due to RMP can be roughly classified by two cases. One is shown in Figure 3.5(a) which is occurred by the decrease of the toroidal rotation speed and the density when RMP is applied, resulting the H-L back transition and subsequent disruption. This type of locking characteristic can be seen in H-mode plasmas. Lots of plasma locking phenomena can be classified into this type in KSTAR ELM control experiments.

The other type of the plasma locking is shown in Figure 3.5(b) which indicates that sufficiently large RMP current in low density L-mode plasmas can make the plasma destabilization and disruption. Most of the plasma locking in this case was occurred by n = 1 RMP. It is noteworthy that the plasma locking by n = 2 RMP was caused in only a few discharges.

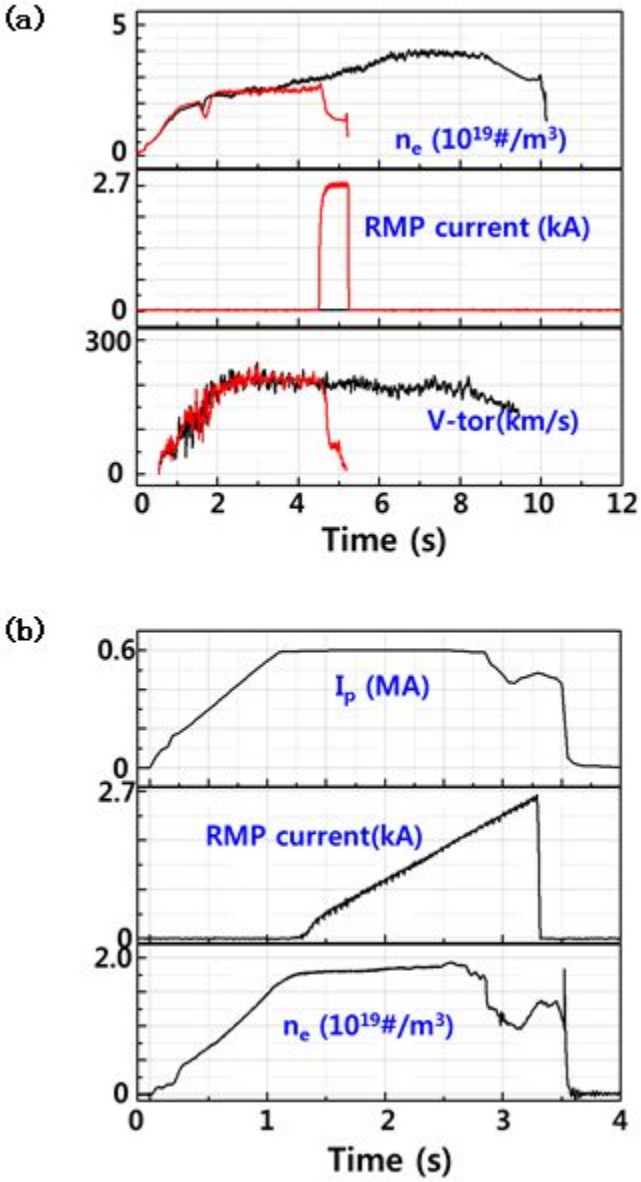

Figure 3.5 Two cases of plasma locking: (a) Locking with H-L back-transition and subsequent disruption when RMP applied in H-mode plasmas (#9063) which is compared with a no RMP case (#9064), (b) Locking over threshold RMP coil current in L-mode plasmas (#8856)

3.2.3 Several features of locked plasmas

The characteristics of locked plasma about the case of Figure 3.5(b) with n = 1 RMP applied shots was investigated since this case was expected to have more effect on the low density limit. Similar investigation was made with n = 1 and n = 2 mixed RMP[15].

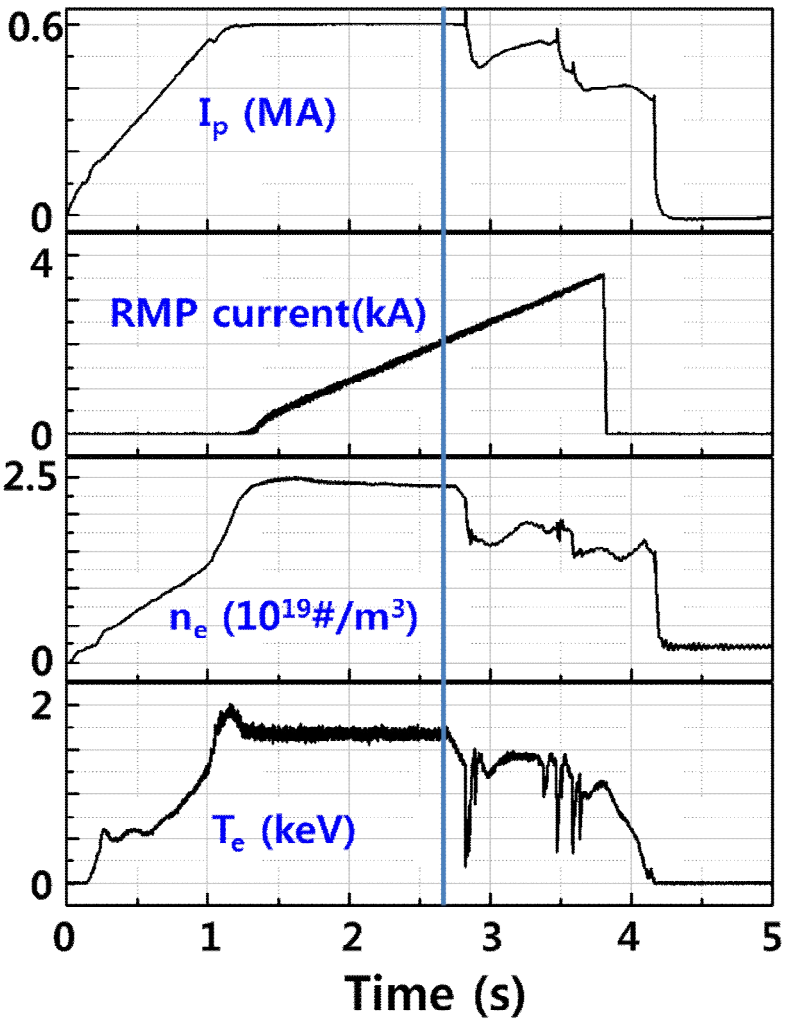

Figure 3.6 Oveview of #8973 with plasma locking point

The typical shot #8973 was chosen and analyzed. The overview of the #8973 is shown in Figure 3.6 where the plasma locking time is vertically indicated. In the reference case the locking threshold was defined by the change of the toroidal rotation velocity and the electron temperature. Unfortunately, the experiments used in this case did not have the toroidal rotation velocioty, so the threshold by the change of electron temperature is thought as the plasma locking point.

When the RMP coil current is increased and reached the threshold value, the electron temperature drops first. And the plasma is

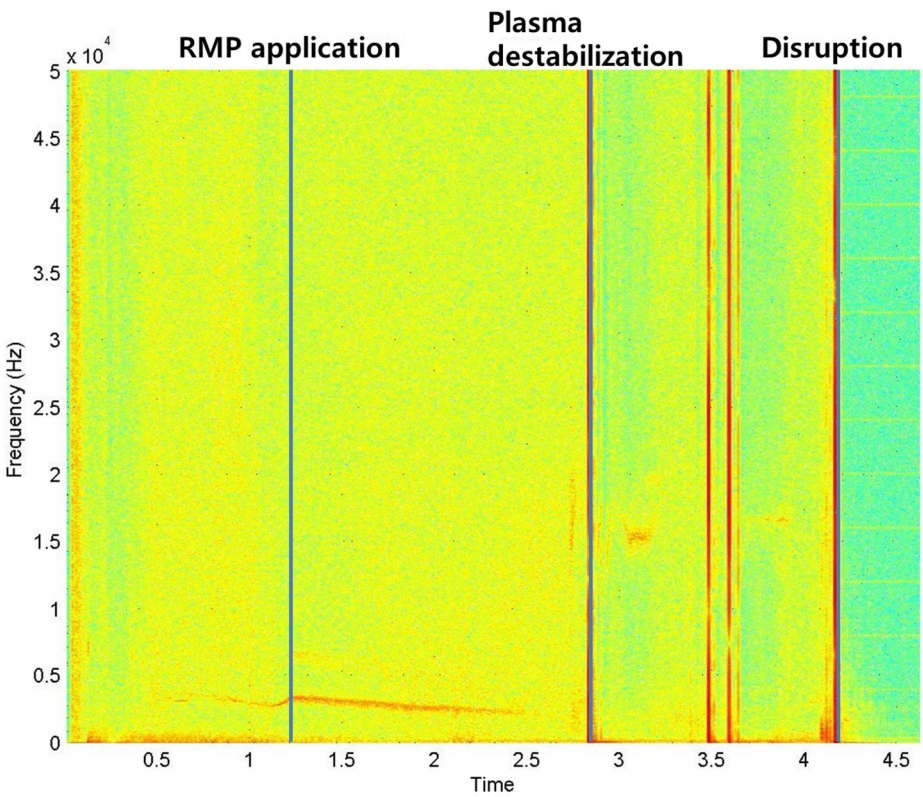

Figure 3.7 MHD spectrogram of #8973

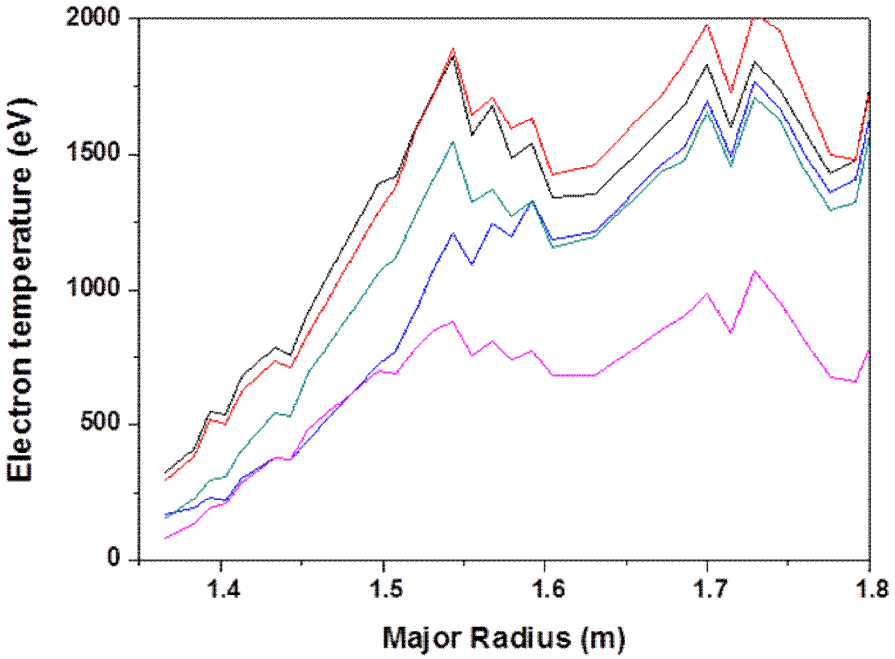

Figure 3.8 Evolution of the temperature profile in time; t = 2.4 s (black), t = 2.7 s (red), t = 3 s (blue) t = 3.3 s (green) and t = 3.6 s (magenta)

destablized globally, shown in 2.82 second. The coil current of RMP was about 2.2 kA, applied by the middle coil. In the MHD spectrogram, an n = 1 mode is observed during the RMP is applied.

The temperature profile evolution is shown in Figure 3.8. When the plasma was destabilized, the edge plasma temperature dropped first. This temperature drop affected the whole plasma region, resulting in the global plasma degradation. At 3.6 s, the edge temperature drop was stopped but the core temperature was decreased.

3.2.4 Low density limit by RMP

The low density limit change due to plasma locking by RMP was investigated with respect to the Greenwald density fraction and Hugill diagram. Figure 3.9 shows the points of disrupted plasmas by plasma locking in the Greenwald fraction and the RMP coil current window. From this result, the conditions for determining low density limit by RMP can be categorized as follows.

One of the condition is the position of the applying RMP. In plasma conditions with a similar density, the coil current needed for plasma locking by the middle RMP is about the half of that by the top or

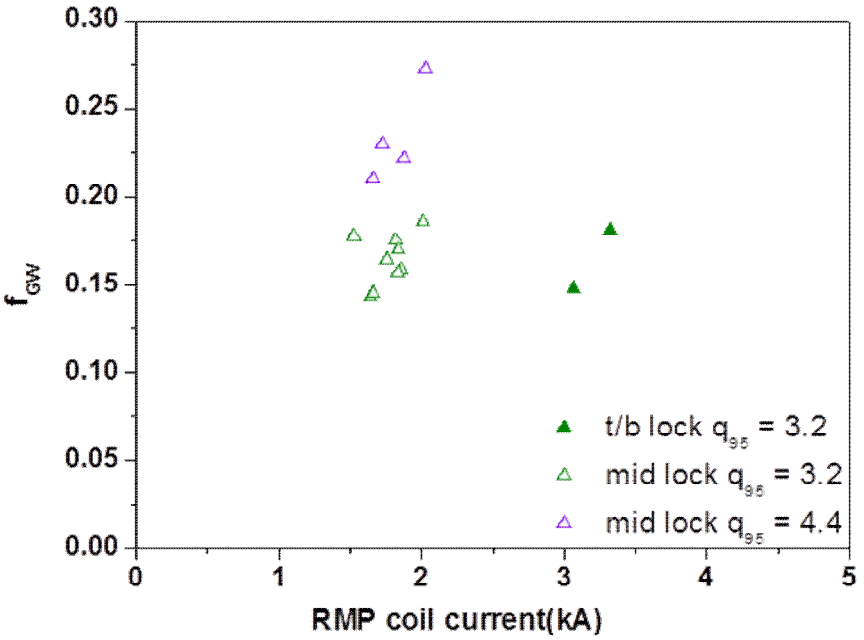

Figure 3.9 Plot of the locking points in Greenwald fraction and RMP coil current window

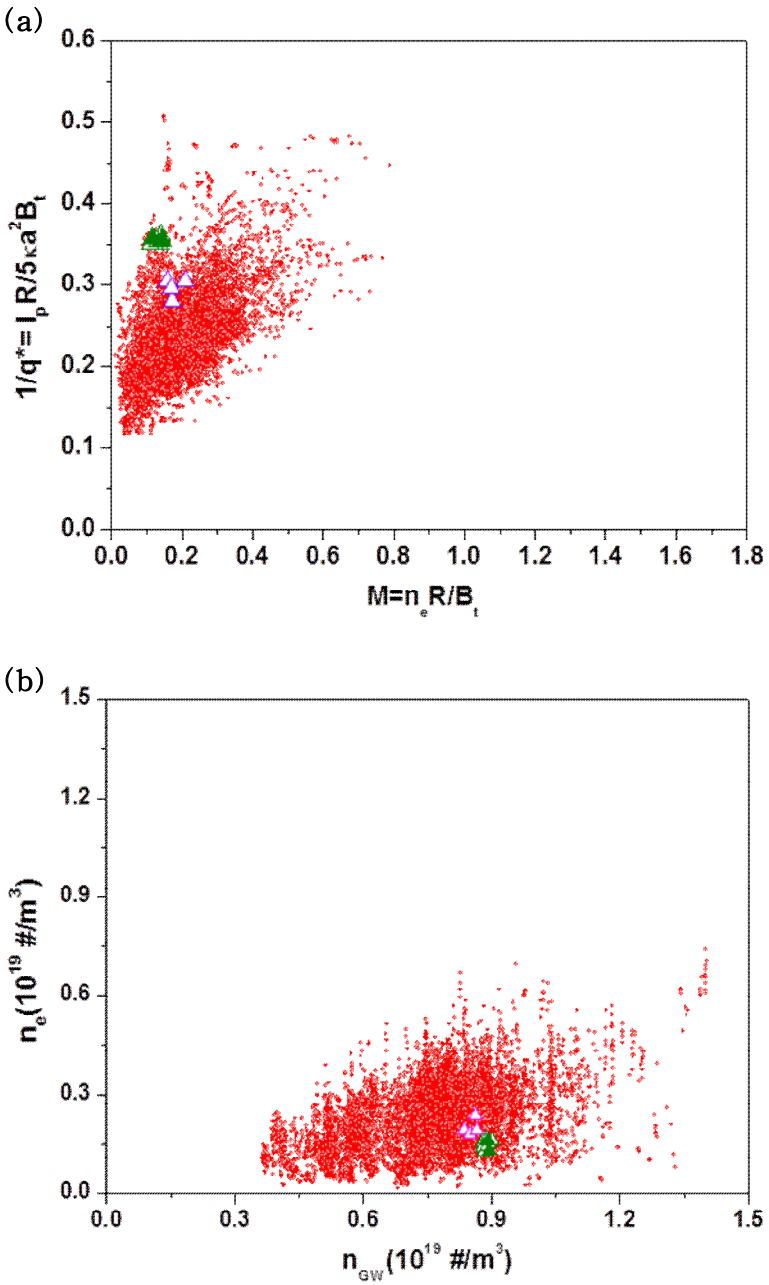

Figure 3.10 Plot of the plasma locking points shown in Figure 3.9 with Hugill diagram and Greenwald fraction diagram

the bottom RMP. This does not appear in Hugill diagram or Greenwald diagram since they do not contain the variable of the RMP coil current. It is expected that if the coil current is the same for all the RMP coils, the low density limit will be much higher for the middle RMP than that for the top or the bottom RMP.

Next the q_{95} value of the plasma seemed to influence the density limit. The plasma shots with $q_{95} = 3.2$ showed the lower density limit than those with $q_{95} = 4.4$. The plasma parameters for $q_{95} = 3.2$ case have I_p = 0.6MA, B_T = 2T and elongation(κ) = 1.6, and for $q_{95} = 4.4$ case have the same I_p and B_T with elongation(κ) = 1.38. So the plasma with low q_{95} or low elongation is thought to exhibit low density limit.

3.2.5 Impact to L-H power threshold by RMP

Finally, Greenwald fraction range of disrupted plasma were applied to L-H threshold plot to investigate the effect of RMP to the L-H transition threshold power [2]. As the density limit in this thesis is treated with Greenwald fraction, the L-H threshold plot was also converted from the line average density to the Greenwald density fraction. The density range of the disrupted plasma is indicated in Figure 3.11 for the two different q_{95} values. As no rt-EFIT data was available for the data, since the rt-EFIT was employed from the middle of 2012 campaign in KSTAR. So the direct comparison is limited here. But it is clearly seen that the low density limit range

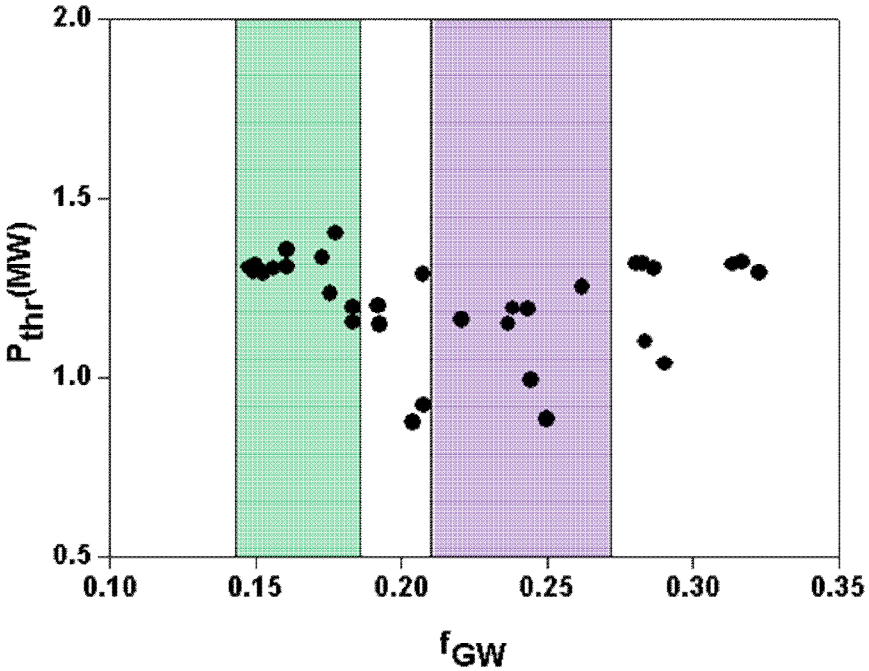

Figure 3.11 Diagram of plasma locking range over L-H threshold power versus Greenwald density fraction for $q_{95} = 3.2$ (green) and $q_{95} = 4.4$ (violet)

set by RMP is in the optimal density range for the lowest L-H transition threshold power to affect L-H transition scenarios.

4. Conclusion

The operation range of KSTAR is investigated in terms of Hugill diagram and the Greenwald density fraction. KSTAR experiments conducted during 4 years were analyzed where 1740 shots were used carefully selected by a data refining process. It is found that KSTAR can reach a far low density range with the achievable Greenwald fraction of 6%.

This accessibility to the low density range is investigated by two main factors known to set the low density limits, the runaway electron and the plasma locking by the error field. It is revealed that the runaway electron does not impact the sustainment of plasma discharges at low density even though significant fraction of the runaway electrons is suspected to present. Instead, increased error field by auxiliary applied RMP can significantly interrupted the plasma discharges resulting in plasma locking and disruption so that access to the low density range was signficantly restricted. The condition for plasma locking by RMP can be differed by the position of RMP and the q_{95} value of the plasma. The higher q_{95} plasma with middle-applied-RMP is expected to have a higher value of low density limit fraction. The impact of the error field increased by RMP is studied for L-H transition. The Greenwald fraction range of the plasma locking seems to cover the optimal density range of the L-H transition point in KSTAR, so caution is needed to design operation scenarios with RMP to suppress edge localized mode in H-mode

plasmas.

This study is mainly done to analyze n = 1 RMP from the middle coil but can be extended to n = 2 RMP and upper/bottom coils which need detailed calculation of the penetrated error field. Comparison of the RMP effect on n = 1 and n = 2 would be interesting and important to prepare ITER where employing RMP is being considered.

References

[1] Martin Greenwald, "Density limits in toroidal plasmas", *Plasma Physics and Controlled Fusion* 44, R27 (2002)

[2] J. -W. Ahn, H. -S. Kim, Y. S. Park, L. Terzolo, W. H. Ko, J. -K. Park, A. C. England, S. W. Yoon, Y. M. Jeon, S. A. Sabbagh, Y. S. Bae, J. G. Bak, S. H. Hahn, D. L. Hillis, J. Kim, W. C. Kim, J. G. Kwak, K. D. Lee, Y. S. Na, Y. U. Nam, Y. K. Oh and S. I. Park, "Confinement and ELM characteristics of H-mode plasmas in KSTAR", *Nuclear Fusion* 52, 114001 (2012)

[3] M. Greenwald, J. L. Terry, S. M. Wolfe, S. Ejima, M. G. Bell, S. M. Kaye, G. H. Neilson, "A new look at density limits in tokamaks", *Nuclear Fusion* 28, 2199 (1988)

[4] M. Murakami, J. D. Callen, L. A. Berry, "Some observations on maximum densities in tokamak experiments", *Nuclear Fusion* 16, 347 (1976)

[5] S.J. Fielding, J. Hugill, G.M. McCracken, J.W.M. Paul, R. Prentice and P.E. Stott, "High-density discharges with gettered torus walls in DITE", *Nuclear Fusion* 17, 1382 (1977)

[6] V.S. Vlasenkov, V.M. Leonov, V.G. Merezhkin and V.S. Mukhovatov, "The runaway electron discharge regime in the Tokamak-6 device", *Nuclear Fusion* 13, 509 (1973)

[7] V.V. Alikaev, K.A. Razumova and Yu.A. Sololov, “Runaway-electron instability in the TM-3 Tokamak ”, *Soviet journal of plasma physics* 1, 546 (1975)

[8] R. S. Granetz, B. Esposito, J. H. Kim, R. Koslowski, M. Lehnen, J. R. Martin-Solis, C. Paz-Soldan, T. Rhee, J. C. Wesley, L. Zeng and ITPA MHD Group, “An ITPA joint experiment to study runaway electron generation and suppression”, *Physics of Plasmas* 21, 072506 (2014)

[9] J. T. Scoville, R. J. La Haye, A. G. Kellman, T. H. Osborne, R. D. Stambaugh, E. J. Strait, T. S. Taylor, “Locked modes in DIII-D and a method for prevention of the low density mode”, *Nuclear Fusion* 31, 875 (1991)

[10] Y. In, J. K. Park, J. M. Jeon, J. Kim and M. Okabayashi, “Extremely low intrinsic non-axisymmetric field in KSTAR and its implications”, *Nuclear Fusion* 55, 043004 (2015)

[11] Y. U. Nam, K. D. Lee, “A 280GHz single-channel millimeter-wave interferometer system for KSTAR”, *Review of scientific instruments* 79, 10E705 (2008)

[12] Y. U. Nam, “Multi-fringe counting technique of millimeter-wave interferometer system for KSTAR”, *Transactions of fusion science and technology* 55, 180 (2009)

[13] H. K. Kim, H. L. Yang, G. H. Kim, Jin-Yong Kim, Hogun Jhang, J. S. Bak, G. S. Lee, “Design features of the KSTAR in-vessel control coils”, *Fusion Engineering and Design* 84, 1029 (2009)

[14] Y. M. Jeon, S. W. Yoon, J. H. Kim, S. H. Hahn, W. C. Kim, Y. K. Oh, Jong-Gu Kwak, W. H. Ko, S. G. Lee, J. G. Bak, K. D. Lee, Y. U. Nam, J. Y. Kim, H. L. Yang, H. K. Kim and KSTAR team, "Aspects and Applications of Non-Axisymmetric Coils on KSTAR", *16th workshop on MHD Stability Control*(USA, 2011)

[15] J. Kim, Y. In, G. Kim, J. Y. Kim, J. G. Bak, Y. Park, G. Yun, J. Seol, S. A. Sabbagh and the KSTAR team, "Disruption threshold of error-field-induced locked mode under n=1 and n=2 mixed non-axisymmetric fields", *25th IAEA Fusion Energy Conference*(Russia, 2014) EX/P8-4 (2014)

국문초록

토카막의 운전조건은 핵융합 출력과 플라즈마 운전 시나리오에 영향을 주기 때문에, 각 토카막의 운전영역을 아는 것은 중요한 연구주제이다. 이 논문에서는 한국형 토카막 장치(KSTAR)에서의 운전영역을 Hugill 도표와 Greenwald 밀도 비율 도표를 바탕으로 분석해 보았다. 이 분석을 위해 2011년부터 2014년까지 KSTAR에서 수행된 실험가운데 1740개의 샷들을 골라내었다. Hugill 도표를 통해 KSTAR의 운전영역을 DIII-D의 운전영역과 비교해 봄으로서, KSTAR는 상당히 낮은 밀도까지 도달할 수 있음을 발견하였으며, 이를 통해 KSTAR가 상당히 낮은 자체 오차장을 가지고 있음을 주장할 수 있다. 현재의 데이터베이스를 바탕으로 했을 때 KSTAR의 도달 가능한 Greenwald 비율의 범위는 6%에서 60%로 나타나는 것으로 보였다.

저밀도 운전 영역을 변화시킬 수 있는 두 가지 요인인 이탈 전자와 오차 장에 대한 효과를 조사하였다. KSTAR에서의 의도된 이탈전자 발생 실험을 바탕으로 이탈전자의 발생에 대한 조건이 Dreicer 조건을 바탕으로 조사되었다. 비록 이 실험들이 이탈전자를 발생시키기에 충분한 조건을 가졌지만, 이 샷들은 중대한 방해가 없이 지속될 수 있었다. 이 관찰을 통해 이탈 전자는 KSTAR에서의 저밀도 운전 제한에 영향을 주는 주 요인이 아닌 것으로 보인다. 반면에, 자기공명섭동(RMP)이 들어감으로 인해 오차장이 증가한 플라즈마 샷들은 종종 플라즈마 잠김 현상을 나타내었고 저밀도 운전영역의 접근이 심각하게 제한되었다. 플라즈마 잠김 임계점은 인가된 RMP코일과 q_{95}값에 의해 변화되는 것으로 발견되었다. 중간 코일에서 플라즈마 잠김을 일으키기 위한 RMP 코일 전류의 크기는 상부나 하부의 코일에서 인가되는 것에 비해 절반

정도의 크기로 나타났다. 그리고 낮은 q_{95}의 값을 가질수록 낮은 밀도에서의 운전이 가능함을 보였으며, $q_{95}=3.2$에서는 $f_{GW}\approx 0.16$로 나타났고 $q_{95}=4.4$에서는 $f_{GW}\approx 0.22$로 나타났다. 저밀도 영역에서의 RMP의 영향이 L-mode에서 H-mode로의 전이에 필요한 외부 인가 출력의 관점에서 조사되었으며, L-H의 효과적인 운전 영역으로의 접근이 RMP 인가에 의해 제한될 수 있음을 보였다. 따라서, 토카막에서 H-mode에서 RMP를 활용할 때에 이 효과를 고려해서 운전 시나리오를 구성해야 할 것을 제안하는 바이다.

주요어 : KSTAR, 밀도 제한, Hugill 도표, Greenwald 밀도 비율, 자기공명섭동, 이탈 전자, 토카막 운전

학 번 : 2013-23182